Differential-flow-induced transition of traveling wave patterns and wave splitting

Shyamolina Ghosh, Shibashis Paul, and Deb Shankar Ray*
Indian Association for the Cultivation of Science, Jadavpur, Kolkata-700032, India
(Received 3 August 2016; revised manuscript received 5 October 2016; published 26 October 2016)

We have analyzed the differential flow-induced instability in the presence of diffusive transport in a reaction-diffusion system following activator-inhibitor kinetics. The conspicuous interaction of differential flow and differential diffusivity that leads to pattern selection during transition of the traveling waves from stripes to rotating spots propagating in hexagonal arrays subsequent to wave splitting has been explored on the basis of a few-mode Galerkin scheme.

DOI: 10.1103/PhysRevE.94.042223

I. INTRODUCTION

Pattern formation, or self-organized structures in active media, has been an interesting area of research over the past few decades [1–4]. One of the fundamental mechanisms of pattern formation under far-from-equilibrium conditions is Turing instability, which arises due to interaction between a chemical reaction and diffusion [5]. This instability can occur in systems with activator-inhibitor kinetics where the diffusion coefficient of the inhibitor exceeds that of the activator leading to stationary patterns. The Turing pattern has been observed experimentally [6–10] in chemical systems, and it remains fundamental as a basis for biological morphogenesis [11–13] and in several areas of physical and chemical sciences [14–17]. In a related context, Rovinsky and Menzinger [18,19] demonstrated an alternative mechanism of disengaging the key species, namely the activator and the inhibitor, by making use of differential flow rather than differential diffusivity. This leads to differential flow-induced chemical instability giving rise to spatiotemporal patterns.

The central theme of the paper concerns differential flow-induced instability in the presence of diffusive transport. The differential flow may be realized and controlled in a number of ways. For example, in the case of ionic species, it is possible to apply an external electric field of appropriate strength [20–24]. An electric field has been shown to have a profound influence on the structure changes by induced flow from stationary to time-dependent behavior [20]. A transition from stationary hexagonal Turing patterns to spots moving parallel to the direction of the applied field has been observed in a chlorine dioxide-iodine-malonic acid system [21]. It has been shown that waves can be reversed and even be subjected to splitting in excitable media by an electric field [22]. Electrodiffusion in the layer adjacent to the cell membrane has been modeled to demonstrate dispersion instability and spatiotemporal patterning [23]. Spinning propagation of diffusively unstable planar fronts has been demonstrated in an autocatalytic reaction-diffusion-advection system with cubic kinetics [25]. Since the biological cells and organs remain in the fluid stream, differential flow can also be effected through convection. This has been implemented in modeling the peroxidase-oxidase enzyme reaction mechanism [26]. Differential shear flow can affect pattern formation in a cubic autocatalytic reaction [27]. Another way to implement differential flow is to use a pressure gradient in the fluid medium, since by Darcy's law velocity is proportional to the pressure gradient so long as the gradient is not too large [28,29]. As the spatiotemporal patterns in the form of traveling waves underlie the transmission of information, growth, and development processes as possible mechanisms in living organisms and cells [30,31], differential flow and differential diffusivity play an important role in determining the nature of instability.

Although the scope of the various spatiotemporal scenarios mentioned above is very broad, their primary emphasis lies in linear stability analysis. It is well known that exponential divergence of the unstable mode ultimately gets saturated by the nonlinearity of the dynamics. As the principle of superposition does not work in the nonlinear regime, the dynamical system depending on the symmetry opts for the choice of a few modes. These modes are actually responsible for pattern selection. A major focus of the present paper is to explore this nonlinear state when the homogeneous stable state of the reaction-diffusion system is subjected to differential flow-induced instability. As the analytical solution of the reaction-diffusion-advection equation is impossible, one often resorts to the amplitude equation technique [32,33], which is widely used in related issues. That method, however, is limited by weak nonlinearity and a near-threshold condition. A simpler alternative is to employ the Galerkin model, in which the partial differential equations are replaced by a set of ordinary nonlinear differential equations for a few modes [34,35], in the spirit of the Lorenz equations derived from the Navier-Stokes equation in fluid mechanics [36,37]. The choice of these modes and their stability conditions reflect the nature of the pattern. In what follows, we consider a reaction-diffusion system with activator-inhibitor kinetics due to the Gierer-Meinhardt model in developmental biology [38,39]. We show that differential flow-induced instability results in a traveling wave pattern beyond a critical flow velocity and in wave splitting, yielding propagating spots arranged as hexagonal arrays at higher flow velocities. Specifically, our aim here is (i) to understand the nature of the underlying nonlinear state with the help of Galerkin analysis, (ii) to explore the transition of traveling wave patterns from stripes to spots subsequent to wave splitting, and (iii) to understand the conspicuous interaction between differential flow and differential diffusivity in the dynamics of wave splitting.

*Corresponding author: pcdsr@iacs.res.in

 ©2016 American Physical Society

The rest of the paper is organized as follows: In Sec. II, we discuss the aspects of linear stability analysis of the Gierer-Meinhardt model, followed by numerical simulation of the associated reaction-diffusion equation in the presence of differential flow. Galerkin analysis of the instability in dealing with the nonlinear state is carried out in Sec. III. The paper is concluded in Sec. IV.

II. DIFFERENTIAL FLOW-INDUCED INSTABILITY IN THE PRESENCE OF DIFFUSIVE TRANSPORT

A. Gierer-Meinhardt model and linear stability analysis

We consider a simple activator-inhibitor kind of model proposed by Gierer and Meinhardt [38] in the context of morphogenesis. The activator (u) and inhibitor (v) species undergo a chemical reaction and at the same time diffuse without being subjected to any severe restriction of the Turing condition for instability of the homogeneous steady state. In addition, we assume that the species experience differential transport due to the imposition of a flow term in the dynamics of the activator. The reaction-diffusion-flow equations for the system are given by

$$\dot{u} = \left(\frac{u^2}{v} - u + \sigma\right) + D\nabla^2 u + V\frac{\partial u}{\partial x}, \tag{2.1}$$

$$\dot{v} = \mu(u^2 - v) + \nabla^2 v. \tag{2.2}$$

Here, σ is the rate of formation of the activator, μ is the rate of removal of the inhibitor due to interaction, D is the ratio of the diffusivities of the activator to the inhibitor, and V is the flow velocity of the activator. The dynamical system (2.1) and (2.2) admits a homogeneous steady stable state $[u_0 = (1+\sigma), v_0 = (1+\sigma)^2]$. The stability requires the condition $\mu > \mu_c$, with $\mu = \mu_c [= (\frac{1-\sigma}{1+\sigma})]$ referring to the Hopf line, which separates the homogeneous steady state from the unstable oscillatory state. Furthermore, it is also well known from the linear stability analysis that in the absence of the flow term, diffusion-driven instability comes into play when the homogeneous steady state becomes unstable for the Turing condition $\mu = \frac{1}{D}\left(\sqrt{\frac{2}{1+\sigma}} - 1\right)^2$. In Fig. 1, we plot the Hopf and Turing critical lines to depict the regions of instability that separate out the homogeneous stable steady-state region from the homogeneous oscillatory state and the inhomogeneous patterned state. For further analysis, we have chosen the point P in μ-D space (for $V = 0$) in the homogeneous steady-state region for $\sigma = 0.2$.

Having identified the Hopf and Turing instability regions, we now analyze the flow-induced instability of the steady state P as shown in Fig. 1. Toward that end, linearization of the system near this steady state (u_0, v_0) yields

$$\begin{pmatrix}\dot{\delta u}\\ \dot{\delta v}\end{pmatrix} = \mathbf{A}\begin{pmatrix}\delta u\\ \delta v\end{pmatrix} + \begin{pmatrix}D & 0\\ 0 & 1\end{pmatrix}\begin{pmatrix}\nabla^2\delta u\\ \nabla^2\delta v\end{pmatrix} + \begin{pmatrix}V\\ 0\end{pmatrix}\begin{pmatrix}\partial_x(\delta u)\\ \partial_x(\delta v)\end{pmatrix}, \tag{2.3}$$

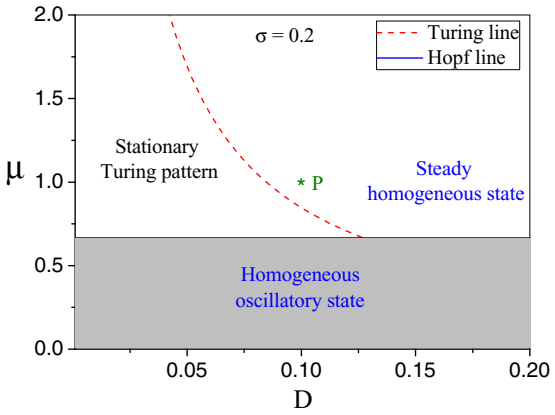

FIG. 1. Phase diagram corresponding to linear stability analysis of Eqs. (2.1) and (2.2) in the absence of the flow term; $V = 0.0$ (arb. units). Hopf (solid blue) and Turing (dashed red) lines are shown to divide the parametric space into a steady homogeneous region, an oscillatory homogeneous region, and a stationary Turing pattern region.

where

$$\mathbf{A} = \begin{pmatrix}a_{11} & a_{12}\\ a_{21} & a_{22}\end{pmatrix} = \begin{pmatrix}\frac{2u_0}{v_0} - 1 & -\frac{u_0^2}{v_0^2}\\ 2\mu u_0 & -\mu\end{pmatrix} \tag{2.4}$$

and $u = u_0 + \delta u$, $v = v_0 + \delta v$. Considering our two-dimensional (2D) system to be periodic, we use a spatial Fourier expansion of the perturbations $\delta u(\vec{r},t) = e^{\lambda t}\int \delta u_K e^{i\vec{K}\cdot\vec{r}}\, d\vec{K}$ and $\delta v(\vec{r},t) = e^{\lambda t}\int \delta v_K e^{i\vec{K}\cdot\vec{r}}\, d\vec{K}$ to derive the eigenvalue equation with growth rate λ and wave vector $\vec{K}$,

$$\begin{vmatrix} a_{11} + ikV - DK^2 - \lambda & a_{12}\\ a_{21} & a_{22} - K^2 - \lambda\end{vmatrix} = 0, \tag{2.5}$$

where we have abbreviated $K^2 = k_x^2 + k_y^2$ and $k_x = k$. The eigenvalues ($\lambda_\pm$) of the system are given by

$$\lambda_\pm = \tfrac{1}{2}[\mathrm{Tr}(\mathbf{M}) \pm \sqrt{\mathrm{Tr}(\mathbf{M})^2 - 4 \mid \mathbf{M} \mid}] \tag{2.6}$$

with

$$\mathrm{Tr}(\mathbf{M}) = (a_{11} + a_{22}) - (D+1)K^2 + ikV \tag{2.7}$$

and

$$|\mathbf{M}| = [\mathrm{Det}(\mathbf{A}) - (a_{11} + a_{22}D)K^2 + DK^4 + ikV(a_{22} - K^2)]. \tag{2.8}$$

The expression for the growth rate $\mathrm{Re}(\lambda_\pm)$ is given by

$$\mathrm{Re}(\lambda_\pm) = \frac{1}{2}\left[a_{11} + a_{22} - (D+1)K^2 \pm \frac{1}{\sqrt{2}}\sqrt{R + \sqrt{R^2 + S^2}}\right], \tag{2.9}$$

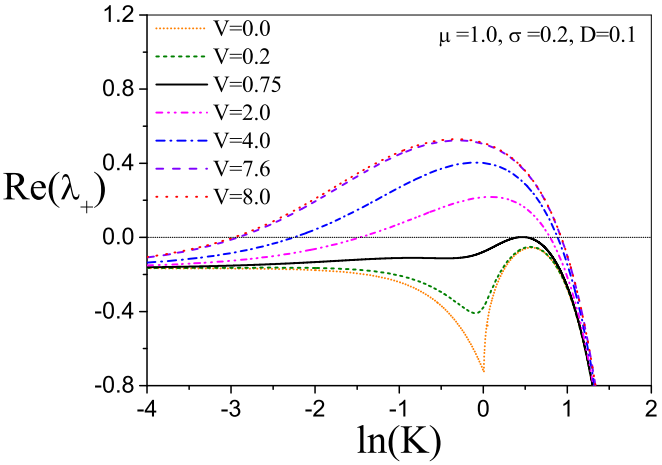

FIG. 2. Dispersion relation for flow-induced instability in the presence of diffusion; plot of the real part of the eigenvalue $\mathrm{Re}(\lambda_+)$ vs $\ln(K)$ at different flow velocities for $\sigma = 0.2$ for the chosen homogeneous steady state P of Fig. 1 with $\mu = 1.0$, and $D = 0.1$ (arb. units).

where

$$R = [(a_{11} - a_{22}) - (D-1)K^2]^2 + 4a_{12}a_{21} - k^2V^2, \quad (2.10)$$

$$S = 2kV[(a_{11} - a_{22}) - (D-1)K^2]. \quad (2.11)$$

In Fig. 2 we plot the growth rate $\mathrm{Re}(\lambda_+)$ of perturbation on the homogeneous stable steady state $P(\mu = 1.0, D = 0.1)$ with $\sigma = 0.2$ against $\ln(K)$ for several values of the flow velocity V. As the flow is considered to be present only in the x direction, the wavelength along the y direction is too long compared to the system size, so that $k_y \sim 0$. When $V = 0.0$, $\mathrm{Re}(\lambda_+)$ remains negative. As the flow velocity is increased, the growth rate begins to increase. At $V = 0.75$, the critical growth rate (solid black line) touches the zero line indicating the flow-induced instability threshold. For V larger than its critical value, we encounter an allowed range of K values corresponding to a positive growth rate $\mathrm{Re}(\lambda_+)$ indicating spatiotemporal inhomogeneity, as represented by the four lines above the solid black line.

B. Numerical simulations; traveling waves and wave splitting

To corroborate the above linear analysis, we carry out a detailed numerical integration of Eqs. (2.1) and (2.2) in two dimensions for several values of the flow velocities. The explicit Euler method following discretization of space and time is used. A finite system size of 30×30 dimensions with periodic boundary conditions has been chosen. A cell size $\Delta x = 0.2, \Delta y = 0.2$ and a time interval $\Delta t = 0.0025$ are set for the present purpose. The results are shown in Fig. 3. Below the critical flow velocity ($V = 0.75$), the system remains homogeneous. At $V = 0.75$, the traveling waves in the form of vertical stripes start propagating along the x direction. Figures 3(a)–3(d) are comprised of four frames taken at an interval of 500 time units, as indicated. The last member (e) of the first column of Fig. 3 exhibits the variation of u along the x direction keeping $y = 15.0$, corresponding to each wave profile of the four snapshots. In the second and third columns of Fig. 3, we display the snapshots of traveling wave profiles of u for higher values of flow velocity $V = 2.0$ and 4.0, respectively. Figure 3 also shows that just at the threshold flow velocity $V = 0.75$, the amplitude of the traveling wave varies initially. Eventually it settles down at a constant amplitude for approximately 8500 time units. At a higher flow velocity beyond threshold, i.e., for higher input energy, when the amplitude is very large the attainment of constancy is observed at a much earlier time, as shown. The relative position of a vertical stripe in the four frames and the spatial gap between the stripes in each frame clearly show that the waves move faster for higher velocities. With a further increase of flow velocity, the stripes start getting fragmented. Such prototypical behavior is shown in Figs. 4(a) and 4(b) for $V = 7.6$. At $V = 8.0$, this wave splitting results in moving spots arranging themselves in the form of a hexagonal lattice. The relative movement of individual spots, which appears like rotating spots, is shown by marking each of them in the four snapshots of Figs. 4(c)–4(f). A pertinent point that needs to be emphasized is that the spots numbered 1–6 do not rotate around a central spot; rather, each of them travels with the flow and also rotates. These rotating spots are reminiscent of an earlier theoretical observation [25] of a spinning front that emerges due to the periodic azimuthal boundary condition on the reaction-diffusion-advection system. The origin of the rotation of the spots in the present case, however, is due to the resultant propagation of concentration flux in the longitudinal and transverse directions. In the longitudinal direction, both convective and diffusive flows operate, while in the transverse direction we have only diffusive motion. In the absence of any transverse diffusion, the rotating spots are not observed.

We now discuss the effect of domain size and boundary conditions on pattern selection. It is known [40] that there is a linear relationship between the flow and the wavelength of the traveling waves generated by the differential flow. Since the wavelength has a crucial dependence on the boundary or confinement of the system, the nature of the pattern is expected to be determined by the boundary conditions. Our numerical simulations of Figs. 3 and 4 are based on a small domain and periodic boundary conditions. The latter implies that the configuration of the quasi-1D-reactor is circular, as considered by several authors [18,19,25,41]. In the circular reactor, the perturbation of the uniform state was imposed as a function of spatial coordinate with an amplitude equal to roughly less than 1% of the steady-state value. In Fig. 5 we have extended our numerical simulations to two larger domain sizes, e.g., with 120×120 (a)–(d) and 300×300 (e)–(h) for the same velocity $V = 8.0$. It has been observed that a smaller grid size facilitates the breakup of traveling waves, while for a larger domain size the traveling waves move with a smaller amplitude and retain their form for the same flow velocity. Application of the zero-flux boundary condition does not lead to the observed phenomena. It is pertinent to mention at this juncture that for reaction-diffusion-advection systems, boundary conditions are often chosen so that at the inlet of the reactor the conditions correspond to a steady state in the feeding chamber, and at the outlet one uses zero flux boundary conditions [42]. The Dirichlet boundary can also be changed for a Danckwerts-type boundary in the inlet [43].

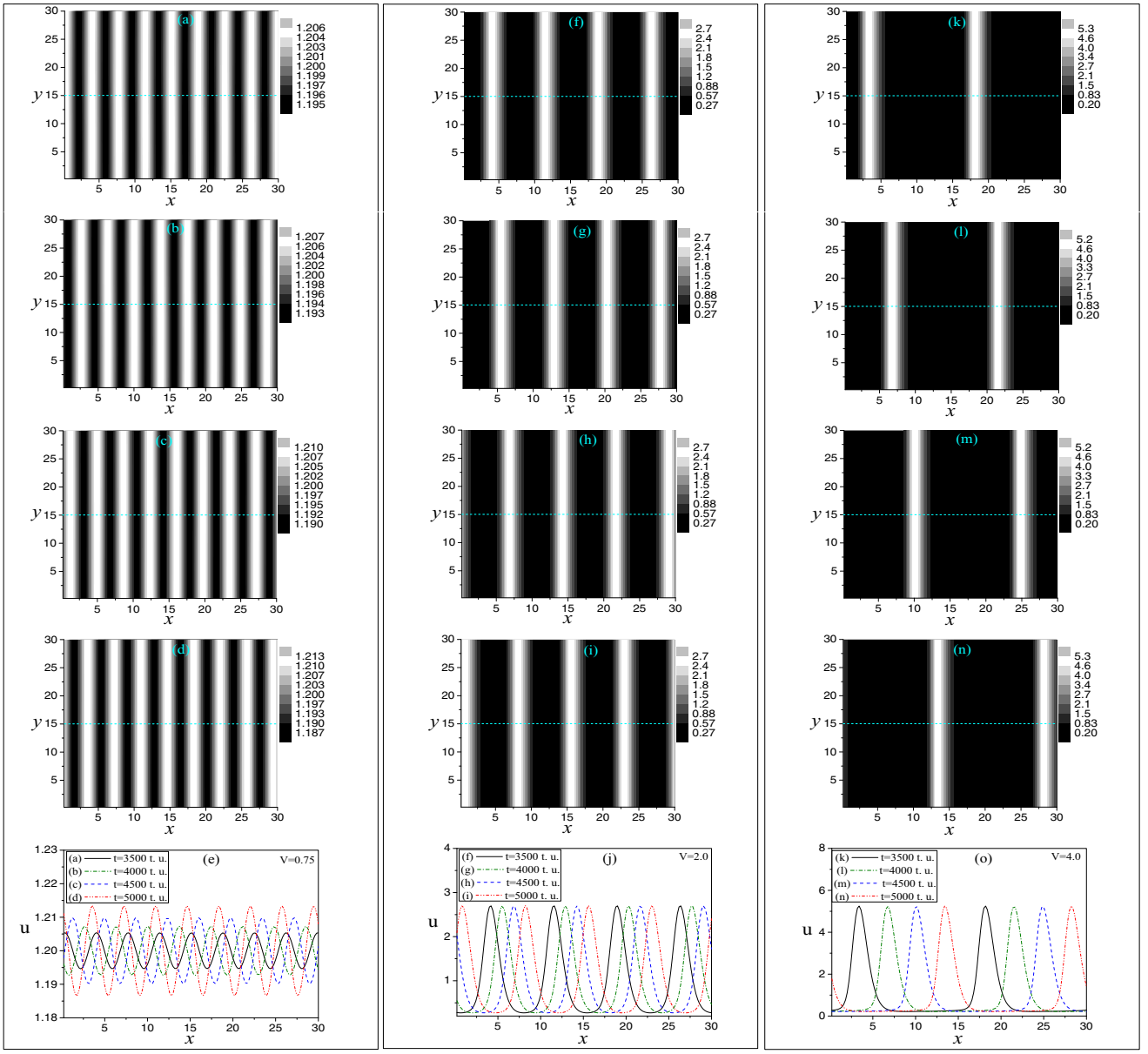

FIG. 3. Numerical simulation of Eqs. (2.1) and (2.2): (a)–(d) Snapshots of traveling stripes of u resulting from instability of state P ($\mu = 1.0$, $D = 0.1$) for $\sigma = 0.2$ and $V = 0.75$ (flow-induced instability threshold as shown in Fig. 2) at time (a) $t = 3500$ t.u., (b) $t = 4000$ t.u., (c) $t = 4500$ t.u., and (d) $t = 5000$ t.u. (arb. units). The last member (e) of the first column represents the variation of u with x for a fixed y at 15.0 for each snapshot. (f)–(i) Same as in (a)–(d) but for $V = 2.0$ (above the instability threshold). The last member (j) of the second column shows that stripes become uniform and move fast. (k)–(o) Same as in (f)–(j) but for $V = 4.0$. Stripes become uniform.

We therefore emphasize that both the domain size and the boundary conditions are important for the traveling waves and their fragmentation. This observation may be rationalized as follows. It is well known [43] that a periodic domain admits a very large number (to be precise, an infinite number) of coexisting periodic solutions with varying wave vectors. When the domain size is relatively small, the waves with a larger amplitude dominate and nonlinear saturation takes over. This leads to the generation of spots after the breakup of traveling waves with a higher amplitude. We shall return to the issue in the next section on Galerkin analysis, which sheds more light on pattern selection through nonlinear interaction.

The occurrence of differential flow-induced instability leading to traveling waves is determined by the magnitude of flow velocity $|V|$. In our numerical simulations, we have maintained the ratio of diffusivities, $D = 0.1$, throughout. We have extended our simulations for the cases in which the ratio is kept at unity, and we observed that the traveling waves can be generated beyond the critical flow velocity. Upon increasing the flow velocity, the stripes undergo splitting in a similar manner, but the fragmented spots do not arrange themselves in regular arrays; rather, they assume randomly scattered irregular structures in the medium. For the sake of brevity, we have not reproduced the results here.

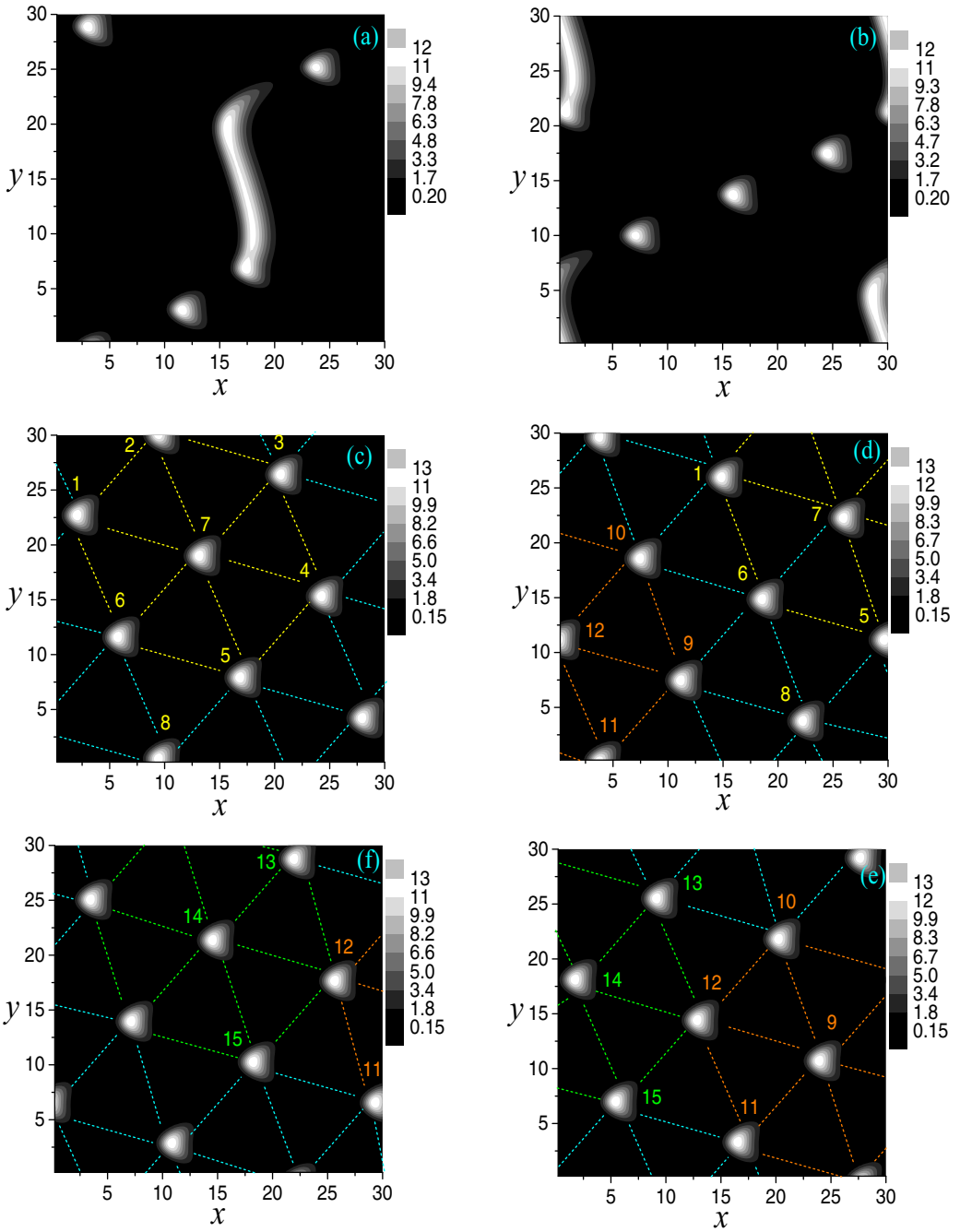

FIG. 4. Wave splitting: (a) and (b) Same as in Fig. 3 but for $V = 7.6$ at time (a) $t = 4500$ t.u. and (b) $t = 5000$ t.u.; traveling stripes get fragmented. (c)–(f) Same as in Fig. 3 but for $V = 8.0$; traveling spots move in hexagonal arrays. The movement of hexagons in time is shown by marking each spot by numbers.

The splitting of traveling concentration waves is reminiscent of an interesting experimental observation of electric-field-induced wave splitting in an excitable medium (the one-dimensional Belousov-Zhabotinsky reaction) [22] by Sevcíková *et al.* It is thus plausible that although the interaction between the chemical reaction, diffusion, and transport of species is important, fluid convection is very much involved in the process of wave splitting, since this splitting was observed only in the experiments in liquid systems in rectangular confinement, and concentration gradients appear in the direction of flow [22]. In summary, we may conclude from our numerical study that both differential flow and differential diffusivity are important for the traveling waves to exhibit splitting beyond a critical threshold velocity, leading to the formation of spots moving in the direction of flow velocity, in hexagonal arrays.

A closer look at the formation of traveling waves in the form of vertical stripes moving along the direction of flow velocity and their transformation to traveling spots subsequent to wave splitting at high flow velocity clearly indicates that while the

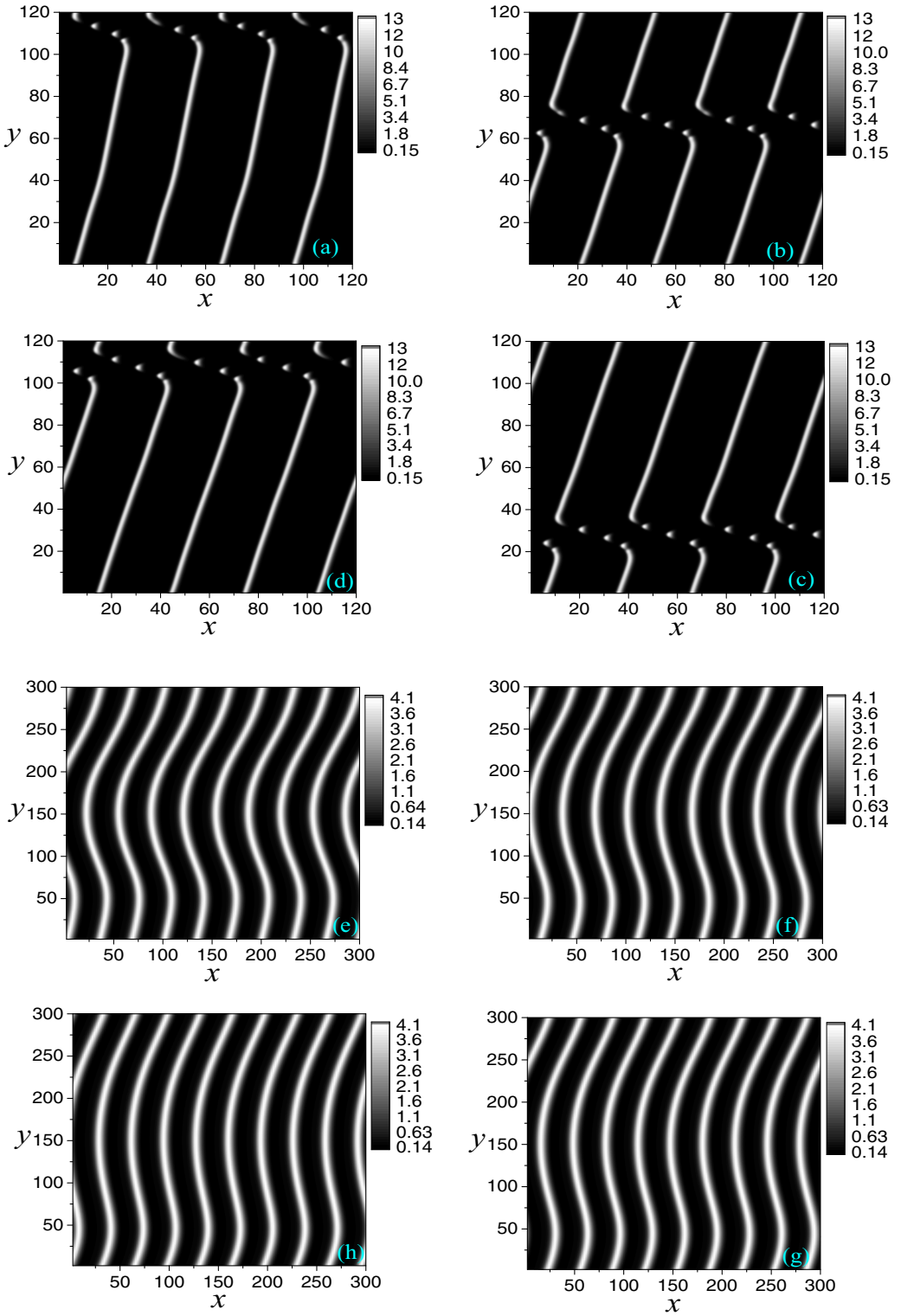

FIG. 5. Effect of domain size: (a)–(d) Same as in Fig. 3 but for $V = 8.0$ and domain size 120×120; traveling stripes get fragmented. (e)–(h) Same as in (a)–(d) but for domain size 300×300 and $\Delta x = 2.0$. No fragmentation is observed as the amplitudes of the waves are small.

vertical stripes are due to the formation of spatial nodes along the x direction, the spots are generated as a result of the formation of nodes along both the longitudinal and transverse directions. This transformation of stripes to spots is therefore associated with a crossover of pattern types, and it depends on the underlying nonlinear state of the system. We implement Galerkin models used for exploring this state. In the next section, we replace the reaction-diffusion-advection equations (2.1) and (2.2) with a set of ordinary nonlinear differential equations for a few judiciously chosen modes by inspection.

The nature of the pattern formation can be ascertained by the stability analysis of these modes.

III. GALERKIN ANALYSIS OF TRAVELING WAVES AND WAVE SPLITTING

In general, inhomogeneity, whether it is stationary or oscillatory, arises due to unstable modes of a given perturbation on the initial stable steady state of the homogeneous system. Depending on the unstable modes along any particular direction, we see stripes, spots, or any other pattern as the case may be. The Galerkin method helps us to understand the nature of these patterns by keeping the number of modes to a minimum. We start with two exact concentration variables u and v, which are expanded in terms of a series of orthogonal basis functions representing the spatial structure of the concentration profile, whereas the combining coefficients determine the relative weight of the profile. The dynamics of the reaction-diffusion-advection system thus reduces to the nonlinear dynamics of these finite-number coefficients or modes. In our case, for analysis of stripes and spots, we choose specifically the following forms of expansions:

$$u(x,y,t) = a_0 + a_1\cos(k_x x) + a_2\sin(k_x x) + a_3\cos(k_x x)\cos(k_y y) + a_4\sin(k_x x)\cos(k_y y), \tag{3.1}$$

$$v(x,y,t) = b_0 + b_1\cos(k_x x)\cos(k_y y). \tag{3.2}$$

For simplicity, we consider $k_x = k_y = k$. This choice is guided by the following numerical consideration. At high flow velocity V when the traveling waves undergo fragmentation generating fully developed spots, as in Figs. 4(c)–4(f), the nodes appear in the x and y directions almost in equal proportion. Now, for a homogeneous state we would have $a_1 = a_2 = a_3 = a_4 = b_1 = 0$, so that the state (u,v) reduces to (u_0,v_0). For $a_3 = a_4 = b_1 = 0$ (but $a_1, a_2 \neq 0$), nodes appear only along the x direction. Therefore, we expect to observe stripes in the x direction. To consider such stripe-patterned states, we put this condition in Eqs. (3.1) and (3.2). The resulting expansions in u and v are then used in Eqs. (2.1) and (2.2). By equating the coefficients of the appropriate Fourier terms on either side, we obtain the following equations of the four coupled modes:

$$\dot{a_0} = \frac{a_0^2}{b_0} + \frac{a_1^2}{2b_0} + \frac{a_2^2}{2b_0} - a_0 + \sigma, \tag{3.3}$$

$$\dot{a_1} = \frac{2a_0a_1}{b_0} - (1 + Dk^2)a_1 + kVa_2, \tag{3.4}$$

$$\dot{a_2} = \frac{2a_0a_2}{b_0} - (1 + Dk^2)a_2 - kVa_1, \tag{3.5}$$

$$\dot{b_0} = \mu\left(a_0^2 + \frac{a_1^2}{2} + \frac{a_2^2}{2} - b_0\right). \tag{3.6}$$

Interestingly, the unique steady state of the above four modes is given by

$$a_{0s} = (1+\sigma) = u_0, \quad b_{0s} = (1+\sigma)^2 = v_0, \quad a_{1s} = a_{2s} = 0, \tag{3.7}$$

where the first two terms correspond to a homogeneous steady state. Introducing infinitesimal perturbation δa_0, δb_0, δa_1, and δb_1, where $a_0 = a_{0s} + \delta a_0$, $b_0 = b_{0s} + \delta b_0$, $a_1 = a_{1s} + \delta a_1$, and $b_1 = b_{1s} + \delta b_1$ on the aforementioned steady state in Eqs. (3.3)–(3.6), we obtain the following set of four linearized dynamical equations, which are now decoupled into two sets:

$$\delta\dot{a_0} = \left(\frac{1-\sigma}{1+\sigma}\right)\delta a_0 - \left(\frac{1}{1+\sigma}\right)^2\delta b_0, \tag{3.8}$$

$$\delta\dot{b_0} = 2\mu(1+\sigma)\delta a_0 - \mu\delta b_0, \tag{3.9}$$

and

$$\delta\dot{a_1} = \left(\frac{1-\sigma}{1+\sigma} - Dk^2\right)\delta a_1 + (kV)\delta a_2, \tag{3.10}$$

$$\delta\dot{a_2} = (-kV)\delta a_1 + \left(\frac{1-\sigma}{1+\sigma} - Dk^2\right)\delta a_2. \tag{3.11}$$

The dynamics of δa_0 and δb_0 does not involve D or V and thus represents the oscillatory state. The other set takes care of both diffusion and flow velocity. Assuming δa_1 and δa_2 vary as $\sim e^{\eta t}$, we find the eigenvalues (or growth rate of the given perturbation) as

$$\eta_{\pm(\text{stripe})} = \left(Dk^2 - \frac{1-\sigma}{1+\sigma}\right) \pm i(kV). \tag{3.12}$$

Spatiotemporal instability of the steady state arises when $\text{Re}(\eta_\pm) > 0$ for a finite V. When $k^2 = k_c^2$, i.e., for the critical wave vector corresponding to $V = 0.75$, the homogeneous system as shown in Figs. 2 and 3(a)–3(d) becomes unstable. With $k^2 \geqslant k_{c(\text{stripe})}^2$ $[=(1-\sigma)/D(1+\sigma)]$, the vertical stripes move along the x direction as depicted in Figs. 3(a)–3(o). The spatiotemporal instability leading to the formation of traveling waves in the form of stripes is therefore clearly evident from the eigenvalue $\eta_{\pm(\text{stripe})}$. The appearance of both differential flow (V) and differential diffusivity (D) points toward the interaction of convection and diffusion.

For $a_1 = a_2 = 0$, nodes appear in both the x and y directions, so that one expects spots instead of stripes. To consider this situation, we put this condition in Eqs. (3.1) and (3.2) and proceed as before to obtain the following equations of five coupled modes:

$$\dot{a_0} = \frac{a_0^2}{b_0} + \frac{a_3^2}{4b_0} + \frac{a_4^2}{4b_0} - a_0 + \sigma, \tag{3.13}$$

$$\dot{a_3} = \frac{2a_0a_3}{b_0} - (1 + 2Dk^2)a_3 + kVa_4, \tag{3.14}$$

$$\dot{a_4} = \frac{2a_0a_4}{b_0} - (1 + 2Dk^2)a_4 - kVa_3, \tag{3.15}$$

$$\dot{b_0} = \mu\left(a_0^2 + \frac{a_3^2}{4} + \frac{a_4^2}{4} - b_0\right), \tag{3.16}$$

$$\dot{b_1} = 2\mu a_0a_3 - \mu b_1 - 2k^2b_1. \tag{3.17}$$

A further simplification can be made by observing that b_1 decays much faster so that one can drop the mode b_1 and have a four-mode description that has the same structure. The condition for spatiotemporal instability can be obtained by stability analysis of the steady state corresponding to the

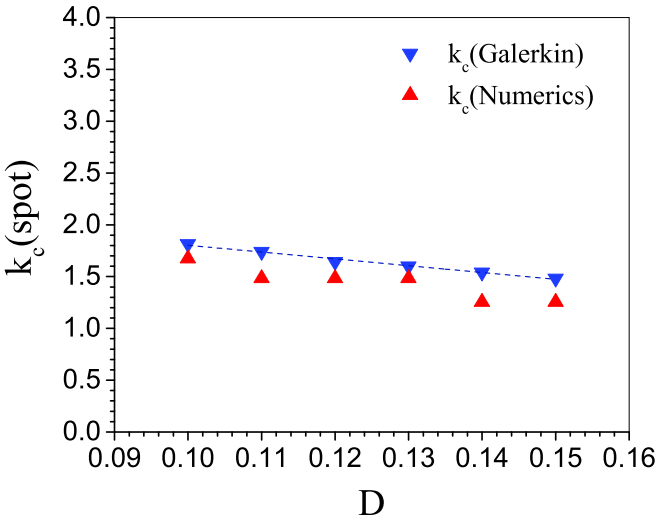

FIG. 6. Variation of the critical wave number $k_{c(\mathrm{spot})}$ for spots as a function of the ratio of the diffusion coefficients, D, for the set of parameters mentioned in the text. A comparison of the theoretical scheme based on Galerkin analysis [Eq. (3.18)] with numerical findings is shown (arb. units).

dynamical system (3.13)–(3.16). This yields the eigenvalues

$$\eta_{\pm(\mathrm{spot})} = \left(2Dk^2 - \frac{1-\sigma}{1+\sigma}\right) \pm i(kV). \qquad (3.18)$$

The instability threshold appears at a critical wave vector $k^2_{c(\mathrm{spot})}$ $[= (1-\sigma)/2D(1+\sigma)]$. This situation corresponds to Fig. 4. In Figs. 4(a) and 4(b) the stripes start splitting, and in Figs. 4(c)–4(f) the rotating spots arrange themselves in hexagonal arrays and travel along the direction of the flow. To describe the onset of wave splitting in terms of wave instability in a more quantitative way, we make use of the results of Galerkin analysis as follows: Eq. (3.18) suggests that the critical wave number for spots is determined by the ratio of diffusion coefficients D, which is varied over a small range as in Fig. 6 for the fixed values of $\sigma(=0.2)$ and μ $(=1.0)$. We then extend our simulation results for these parameter sets just above the critical flow velocity to determine numerically the critical wave number $k_{c(\mathrm{spot})}$ for spots. A comparison between the theoretical and numerical estimates of the critical wave number $k_{c(\mathrm{spot})}$ is shown in Fig. 6. The agreement is fair enough to lend support to our heuristic fixation of transversal wave numbers. The little discrepancy between theory and numerics arises since we used flow velocity a little above the critical flow velocity for the correct counting of nodes after spot formation. The theoretical critical wave number, on the other hand, depends precisely on the critical flow velocity for which spot formation just starts. Finally, the role of differential flow as well as differential diffusivity is quite transparent from the occurrence of V and D in the expressions for the critical wave vectors for spots and stripes. We emphasize two points: First, although instability is flow-induced, differential diffusivity is an important condition for wave splitting. Second, the origin of the wave splitting is somewhat different from that observed in the quasi-one-dimensional BZ reaction [22] as the splitting in the latter case arises as an electric-field-induced effect on a propagating Turing pattern. In the present case, on the other hand, the Turing condition is not maintained.

IV. CONCLUSION

Differential flow-induced instability resulting in the initiation of spatiotemporal pattern formation is based on linear stability analysis of the reaction-diffusion-advection system. The analysis, therefore, cannot capture the nature of patterns and their crossover from one type to another since this depends on the specific nonlinear characteristics of each dynamical system, which becomes more pronounced beyond the critical instability threshold in the long time scale. In the absence of any suitable simple analytical technique, the Galerkin scheme provides an immediate answer to this problem. The present treatment relies on this scheme to ascertain the nature of the nonlinear state responsible for the selection of a specific finite number of modes for each pattern type. The replacement of the partial differential equation, i.e., the reaction-diffusion-advection equation, by a set of ordinary nonlinear differential equations for a few modes corresponding to a definite pattern is therefore worth pursuing. We summarize the main results of this study as follows:

(i) We have analyzed the differential flow-induced instability in the Gierer-Meinhardt model of activator-inhibitor kinetics to show how this instability gives rise to spatiotemporal patterns in the form of traveling waves beyond a critical flow velocity. This is in good agreement with full numerical simulations.

(ii) At a higher flow velocity, the propagating waves of stripe patterns split up to generate spots moving in the direction of flow. This is similar to but not the same as the wave splitting experimentally observed earlier in a Belousov-Zhabotinsky reaction medium in quasi-one-dimensional confinement.

(iii) It has been shown that flow-induced instability results in traveling waves where the Turing restriction of unequal diffusivities is lifted. On the other hand, it has been shown that the conspicuous interplay of differential diffusivity and differential flow is a precondition for wave splitting. The stability analysis of the inhomogeneous Galerkin modes as well as full numerical simulations support this notion.

ACKNOWLEDGMENTS

Thanks are due to the Council of Scientific and Industrial Research, Government of India (S.G.) and for the J. C. Bose National Fellowship (D.S.R.), Grant No. SB/S2/JCB-030/2015, Science and Engineering Research Board, Department of Science and Technology, Government of India for partial financial support.

[1] P. W. Ingham, Nature (London) **335**, 25 (1988); S. B. Carroll *et al.*, Science **265**, 109 (1994).

[2] R. Hoyale, *Pattern Formation: An Introduction to Methods* (Cambridge University Press, Cambridge, 2006).

[3] M. Cross and H. Greenside, *Pattern Formation and Dynamics in Nonequilibrium System* (Cambridge University Press, Cambridge, 2009).

[4] S. Kondo and T. Miura, Science **329**, 1616 (2010).

[5] A. M. Turing, Philos. Trans. R. Soc. London, Ser. B **237**, 37 (1952).

[6] *Experimental and Theoretical Advances in Biological Pattern Formation*, edited by H. Othmer, P. Maini, and J. D. Murray (Springer Science, New York, 1993).

[7] V. Castets, E. Dulos, J. Boissonade, and P. De Kepper, Phys. Rev. Lett. **64**, 2953 (1990).

[8] K.-J. Lee, W. D. McCormick, J. E. Pearson, and H. L. Swinney, Nature (London) **369**, 215 (1994).

[9] D. J. Wollkind and L. E. Stephenson, SIAM J. Appl. Math. **61**, 387 (2000).

[10] J. Horváth, I. Szalai, and P. De Kepper, Science **324**, 772 (2009).

[11] H. Meinhardt, *Models of Biological Pattern Formation* (Academic, London, 1982).

[12] J. D. Murray, *Mathematical Biology: I. An Introduction*, 3rd ed. (Springer, New York, 2001); *Mathematical Biology: II. Spatial Models and Biomedical Applications*, 3rd ed. (Springer, New York, 2003).

[13] L. Edelstein-Keshet, *Mathematical Models in Biology* (SIAM, Philadelphia, 2005).

[14] G. Nicolis, *Introduction to Nonlinear Sciences* (Cambridge University Press, Cambridge, 1995).

[15] I. R. Epstein and J. A. Pojman, *An Introduction to Nonlinear Chemical Dynamics: Oscillations, Waves, Patterns and Chaos* (Oxford University Press, New York, 1998).

[16] S. S. Riaz, S. Kar, and D. S. Ray, J. Chem. Phys. **121**, 5395 (2004); S. S. Riaz and D. S. Ray, *ibid.* **123**, 174506 (2005).

[17] P. Ghosh, S. Sen, and D. S. Ray, Phys. Rev. E **79**, 016206 (2009); S. Ghosh and D. S. Ray, *ibid.* **93**, 032209 (2016).

[18] A. B. Rovinsky and M. Menzinger, Phys. Rev. Lett. **69**, 1193 (1992).

[19] A. B. Rovinsky and M. Menzinger, Phys. Rev. Lett. **70**, 778 (1993).

[20] J. Carballido-Landeira, P. Taboada, and A. P. Muñuzuri, Soft Matter **8**, 2945 (2012).

[21] B. Schmidt, P. De Kepper, and S. C. Müller, Phys. Rev. Lett. **90**, 118302 (2003).

[22] H. Sevcíková, M. Marek, and S. C. Müller, Science **257**, 951 (1992).

[23] A. I. Lobanov, T. Yu. Plyusnina, T. K. Starozhilova, G. Yu. Rfznlchenko, and A. B. Rubin, Biophysics **45**, 483 (2000).

[24] S. S. Riaz, S. Kar, and D. S. Ray, Physica D **203**, 224 (2005); S. Dutta and D. S. Ray, Phys. Rev. E **73**, 026210 (2006).

[25] O. Nekhamkina and M. Sheintuch, Phys. Rev. E **81**, 055204(R) (2010); Chem. Eng. Sci. **63**, 3716 (2008).

[26] B. D. Aguda, J. Chem. Phys. **99**, 5091 (1993).

[27] R. A. Satnoianu, J. H. Merkin, and S. K. Scott, Physica D **124**, 345 (1998); L. Stucchi and D. A. Vasquez, Phys. Rev. E **87**, 024902 (2013).

[28] M. Marlow, Y. Sasaki, and D. A. Vasquez, J. Chem. Phys. **107**, 5205 (1997).

[29] S. Ponce Dawson, A. Lawniczak, and R. Kapral, J. Chem. Phys. **100**, 5211 (1994).

[30] G. G. Matthews, in *Cellular Physiology of Nerve and Muscle* (Blackwell, Oxford, 1986); *Ionic Currents in Development*, edited by R. Nuccitelli (Liss, New York, 1986).

[31] J. Lechleiter. S. Girard, E. Peralta, and D. Clapham, Science **252**, 123 (1991).

[32] M. C. Cross and P. C. Hohenberg, Rev. Mod. Phys. **65**, 851 (1993).

[33] P. Ghosh and D. S. Ray, J. Chem. Phys. **135**, 104112 (2011); O. A. Nekhamkina, A. A. Nepomnyashchy, B. Y. Rubinstein, and M. Sheintuch, Phys. Rev. E **61**, 2436 (2000).

[34] A. Bhattacharyay and J. K. Bhattacharjee, Eur. Phys. J. B **21**, 561 (2001).

[35] P. Ghosh, S. Sen, S. S. Riaz, and D. S. Ray, Phys. Rev. E **79**, 056216 (2009).

[36] D. J. Acheson, *Elementary Fluid Dynamics (Oxford Applied Mathematics and Computing Science Series)* (Clarendon, Oxford, 1990).

[37] L. D. Landau and E. M. Lifshitz, *Fluid Mechanics, Course of Theoretical Physics 6*, 2nd revised ed. (Pergamon, Oxford, 1987).

[38] A. Gierer and H. Meinhardt, Kybernetik **12**, 30 (1972).

[39] A. J. Koch and H. Meinhardt, Rev. Mod. Phys. **66**, 1481 (1994).

[40] R. Tóth, A. Papp, V. Gáspár, J. H. Merkin, S. K. Scott, and A. F. Taylor, Phys. Chem. Chem. Phys. **3**, 957 (2001).

[41] V. Z. Yakhnin, A. B. Rovinsky, and M. Menzinger, J. Phys. Chem. **98**, 2116 (1994).

[42] P. Andresén, M. Bache, E. Mosekilde, G. Dewel, and P. Borckmanns, Phys. Rev. E **60**, 297 (1999); M. Kærn and M. Menzinger, *ibid.* **60**, R3471 (1999); J. R. Bamforth, R. Tóth, V. Gáspár, and S. K. Scott, Phys. Chem. Chem. Phys. **4**, 1299 (2002).

[43] A. Yochelis and M. Sheintuch, Phys. Chem. Chem. Phys. **11**, 9210 (2009).